THE JOURNAL OF PHYSICAL CHEMISTRY A
A JOURNAL OF THE AMERICAN CHEMICAL SOCIETY

pubs.acs.org/JPCA

Article

X-ray-Induced Fragmentation of Isothiocyanic Acid, HNCS

Dorothee Schaffner, Lilith Wohlfart, Katharina Theil, Emil Karaev, John D. Bozek, and Ingo Fischer*

Cite This: J. Phys. Chem. A 2026, 130, 2602−2611

Read Online

ACCESS | Metrics & More | Article Recommendations | Supporting Information

ABSTRACT: We studied the X-ray-induced fragmentation of isothiocyanic acid, HNCS, following core ionization and excitation at the N1s, C1s, and S2p edges by Auger electron−ion coincidence spectroscopy. Mostly similar fragmentation products were identified at the different edges for normal and resonant Auger−Meitner decay, respectively. Upon normal Auger−Meitner decay, the dication was found to dissociate predominantly by C−S bond cleavage into $HNC^+ + S^+$ and $CN^+ + S^+$ ion pairs. The higher yield of undissociated $HNCS^{2+}$ after S2p ionization is explained by a propensity for the population of low-binding energy final states at this edge. Following resonant core excitation into the 13a′ or 4a″ orbital, S^+ was found to be the main fragment, followed by HNC^+. Fragments that require isomerization were observed with low yields after both core ionization and excitation. A comparison to isocyanic acid, HNCO, revealed significant differences in the fragmentation pattern of the two molecules.

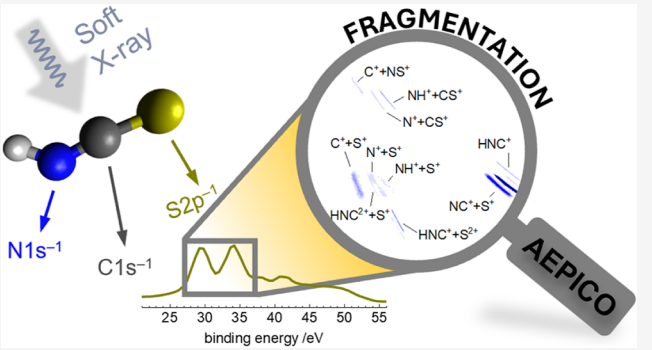

INTRODUCTION

Studying the X-ray-induced fragmentation of isolated molecules is critical to understanding radiation damage in biological systems or the fate of molecules in interstellar space. Soft X-ray irradiation of molecules induces inner-shell ionization or excitation. A core-ionized state of a second- or third-row element deexcites in a normal Auger−Meitner process by ejection of an Auger electron, resulting in a dicationic final state, whereas a neutral core-excited state decays via a resonant Auger−Meitner process that produces the Auger electron alongside a singly charged ion.[1] Both dications and cations are generated in a multitude of (highly excited) electronic states and can subsequently fragment.

In contrast to valence orbitals, inner-shell orbitals in molecules remain localized on their respective atoms, with well-separated ionization and excitation energies for different elements. Consequently, tunable X-ray light sources, such as synchrotrons and free-electron lasers, open up the possibility of selectively creating core holes at different atoms in a molecule.

Here, we present the X-ray-induced dissociation of isothiocyanic acid (HNCS), a tetraatomic molecule with inequivalent atoms that allow for investigation of site-specific fragmentation. Interest in HNCS arises from its detection in different interstellar objects.[2,3] Recent studies have focused on the valence photoelectron spectrum[4] and the fragmentation following single[5] and double[6] photoionization of HNCS. In previous work, we reported the normal and resonant Auger electron spectra at the N1s, C1s, and S2p edges and computationally reproduced decay rates and energetic positions of Auger final states.[7] The present investigation of HNCS by Auger electron-photoion-photoion coincidence spectroscopy reveals additional information about the subsequent fragmentation as well as the dependency of the fragmentation pattern on the binding energy of the corresponding Auger final states. The existence of X-ray sources in space, such as young stars[8] and planetary nebula,[9] motivates this study because fragmentation patterns could be relevant for astrochemical modeling.

X-ray-induced fragmentation dynamics have already been addressed for triatomic molecules related to HNCS, including OCS,[10−12] CS_2,[10,13] and CO_2.[14,15] Furthermore, site-selective fragmentation, i.e., the correlation between the core ionization/excitation site and cleavage of distinct chemical bonds, has been investigated. In an early study on acetone, Eberhardt et al. observed the cleavage of chemical bonds around the core-excited carbon atom and suggested using this effect for selective fission of chemical bonds.[16] Later on, site-selectivity has been observed in small molecules like N_2O,[17,18] O_3,[19] CO_2,[14] and OCS.[11] The impact of nuclear motion in the core-excited/ionized state before the Auger−Meitner decay on the fragmentation was observed, as well as the role of the character of the orbital into which the core electron is excited in resonant processes.[11,15,19] A dependence of the fragmentation

Received: January 19, 2026
Revised: March 4, 2026
Accepted: March 6, 2026
Published: March 12, 2026

on the site of the core hole was also found in larger molecules, e.g., in systems with peptide bonds[20,21] and in halogenated compounds.[22−25] In CH_2BrCl, a comparison to direct valence double ionization showed that the preferred C−Br bond cleavage upon Br3d core ionization is an intrinsic dissociation property of the populated dicationic state and is independent of its generation via core hole decay or double photoionization.[26] The loss of selective fragmentation for dicationic final states at high binding energies was explained by fast internal conversion to lower electronic states in CH_2BrCl^{2+}.[25] The significant role of the internal energy for the fragmentation was pointed out by several studies[27,28] that attribute site-dependent fragmentation patterns to different intensity distributions in the Auger electron spectra, as they correspond to different amounts of internal energy.[24,29] In a combined experimental and theoretical study on ethyl trifluoroacetate, however, similar fragmentation patterns for C1s ionizations at the different carbon atoms were found to result from similar fragmentation properties of the dicationic Auger final states rather than from a fast energy redistribution.[30]

This work extends studies on the reactive tetraatomic molecules isocyanic acid (HNCO)[31,32] and fulminic acid (HCNO).[33,34] In the study on HNCO, several fragmentation pathways were found with similarly high yields, and a preferential N−H bond cleavage was found following N1s ionization. The observation of a rearranged NO^+ product was rationalized by calculations.[32] The Auger electron spectra of isothiocyanic acid and isocyanic acid were found to differ due to the exchange of the chalcogen atom.[7] Here, we investigate the influence of the chalcogen on the concomitant fragmentation pattern.

EXPERIMENTAL METHODS

The experiments were conducted at the soft X-ray beamline PLÉIADES at the synchrotron SOLEIL (Saint-Aubin, France). Isothiocyanic acid was prepared by the reaction of potassium thiocyanate with phosphoric acid, as described previously.[7] The purity of the sample was determined by X-ray absorption (NEXAFS) spectroscopy. The corresponding spectra are included in Section S1 in the SI. The sample was kept at −35 °C and the vapor was introduced effusively into the experimental chamber. The linear, vertically polarized synchrotron light is monochromated by a 600 lines/mm grating before it enters the experimental chamber. The EPICEA setup was used, which is specifically designed for Auger electron−ion coincidence studies.[35] Here, the effusive gas beam is crossed by the photon beam, and the resulting Auger electrons and ions are detected in coincidence in a double toroidal electron analyzer (DTA) that is coupled to an ion time-of-flight (TOF) mass spectrometer. The electrons that are emitted at an angle of 54.7 ± 3°, relative to the light polarization are retarded or accelerated to the pass energy E_P before they are energy-dispersed and detected on a position-sensitive detector (PSD). The width of the energy window of simultaneously detected electrons amounts to 12% E_P, while the resolution is ∼1% E_P.[36] For normal Auger measurements at the C1s and N1s edges and all resonant measurements, a pass energy of 250 eV was used, while for normal Auger experiments at the S2p edge, the pass energy was increased to 300 eV. Each combination of pass energy and acceleration/retardation voltage was adjusted to project the relevant part of the Auger electron spectrum onto the position-sensitive electron detector. For the relation between the radial position r and the kinetic energy E_k of the electron, the empirical formula given in ref 37 was employed. It was calibrated by measuring the known Argon $2p_{3/2}$ and $2p_{1/2}$ photolines with binding energies (E_B) of 248.60 and 250.73 eV.[38] For normal Auger electron spectra (AES), the electron kinetic energy was converted to binding energy by subtracting the kinetic energy from the core ionization energy. For HNCS, we previously determined N1s, C1s, and $S2p_{1/2}$ ionization energies of 405.7, 293.8, and 170.9 eV.[7] In resonant Auger electron spectra (RAES), the binding energy was obtained by subtracting the kinetic energy from the core excitation energy.

When an electron is detected, the coincident ions are extracted from the interaction region with a pulsed electric field. They are analyzed by an ion TOF mass spectrometer and recorded in coincidence with the Auger electron that triggered the extraction pulse. In order to correct for false coincidences, the ion extraction field is additionally pulsed at random intervals. During the measurements, the rate of the randomly triggered pulses was 100/s, while the total number of pulses (including the ones triggered by electron detection) was maintained between 200 and 250/s. The contribution from false coincidences was determined and statistically subtracted according to the procedure described previously[34,39] and in Section S2 in the SI.

RESULTS

Normal Auger-Meitner Processes

Figure 1 shows the TOF mass spectra that were recorded after N1s, C1s, and S2p ionization of HNCS. Because of the shape

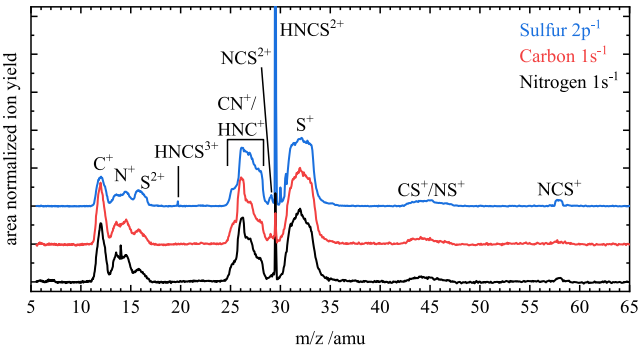

Figure 1. TOF mass spectrum following N1s, C1s, and S2p ionization of HNCS. The $HNCS^{2+}$ signal (m/z 29.5) in the $S2p^{-1}$ spectrum was cut off in order to enhance the visibility of the other ions.

of the extraction pulse, H^+ cannot be detected in the mass spectrometer. All three spectra show a pronounced mass signal at m/z 29.5, which is assigned to the parent dication $HNCS^{2+}$ that is produced by the Auger−Meitner decay after core ionization. The signal is most intense at the S2p edge and decreases significantly for N1s ionization and even more for C1s ionization. At m/z 30, the isotopologue $HN^{13}CS^{2+}$ is visible. A small signal at m/z 19.7 at the S2p edge indicates the formation of $HNCS^{3+}$ by double Auger decay. Here, two valence electrons are ejected when the core hole decays, resulting in a triply ionized final state. Usually, these triply ionized states are dissociative; however, the observation of $HNCS^{3+}$ indicates that its ground state is metastable. This is analogous to the isoelectronic OCS, where a metastable OCS^{3+} is observed after S2p ionization.[40,41] The doubly and triply charged parent ions can dissociate and yield ionic fragments. Compared to the narrow signal of the parent dication, fragment mass signals are broader because of the high kinetic energy release upon dissociation into two charged fragments. The signal at m/z 58 is mainly observed at the N1s and S2p edges and is attributed to an NCS^+ fragment that is produced together with H^+. The weak broad signals around m/z 46 and 44 are assigned to NS^+ and CS^+ based on the photoion−photoion coincidence (PIPICO) map (Figure 2). An intense S^+ signal of a similar magnitude is observed at all three edges. Overlapping mass peaks between m/z 25−28 indicate the

https://doi.org/10.1021/acs.jpca.6c00386
J. Phys. Chem. A 2026, 130, 2602−2611

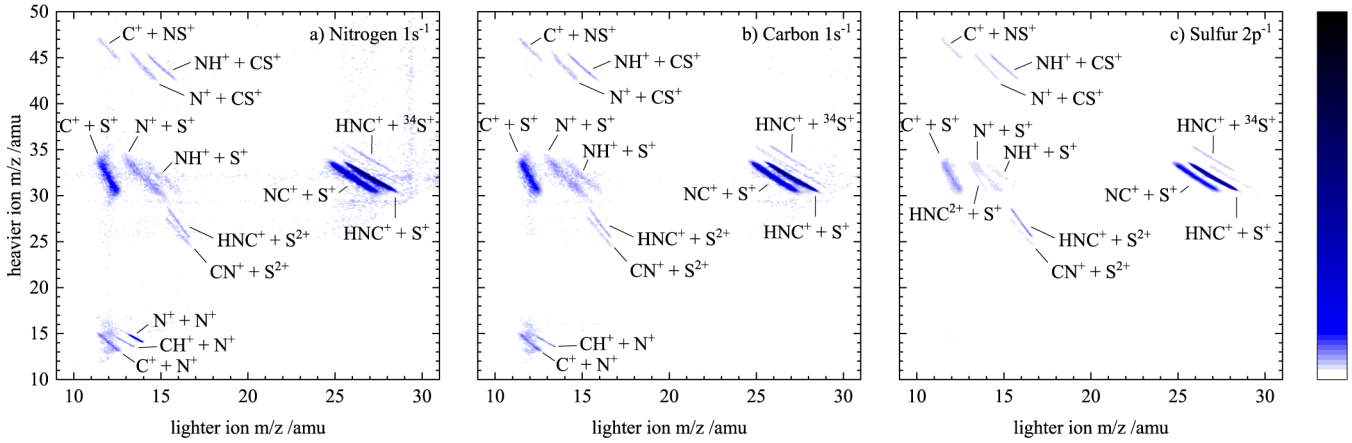

Figure 2. PIPICO map after (a) N1s, (b) C1s, and (c) S2p ionization of HNCS. $CH^+ + N^+$ and $C^+ + N^+$ ion pairs at the nitrogen and carbon edge result (mainly) from an HCN impurity, while $N^+ + N^+$ is formed at the nitrogen edge because of an N_2 impurity.

formation of CN^+ (m/z 26) and HNC^+ or HCN^+ (m/z 27). At the S2p edge, the structure of the signal implies that more HNC^+ is formed than at the other two edges. An HCN impurity from the synthesis and its fragments potentially contribute to the spectrum; however, it can be identified in the PIPICO maps, as will be seen later. The atomic fragments S^{2+}, N^+ and C^+ are present, and the latter two are preferentially formed after C1s and N1s ionization. The broad N^+ signal may also cover NH^+ and CH^+ fragments. A sharp N_2^{2+} peak on top of the broad N^+ signal is attributed to an N_2 contamination.

Figure 2 presents PIPICO maps after N1s, C1s, and S2p ionization. Here, two correlated ionic fragments are detected in coincidence with the same Auger electron. PIPICO maps are used to disentangle overlapping mass signals and to identify ion pairs produced together in the same ionization event. Because of the ions' momentum correlation, ion pairs appear as stripes with a negative slope. Ion pairs resulting from a two-body dissociation of $HNCS^{2+}$, like $HNC^+ + S^+$ and $NH^+ + CS^+$, show a narrow feature with a slope of −1 in time-of-flight units. An additional bond cleavage and the loss of a neutral hydrogen can occur via a concerted or a sequential mechanism.[42] The slightly steeper slope for $CN^+ + S^+$ and $N^+ + CS^+$ suggests a sequential mechanism by secondary dissociation of the initially formed ion pairs. In sequential dissociation, the slope can be deduced from the masses of the neutral and charged fragments.[42] The detection of $C^+ + NS^+$ (slope −1) indicates a rearrangement of the dication because an N−S bond needs to be formed prior to fragmentation. $NH^+ + S^+$ and $N^+ + S^+$ show steeper slopes that do not match a single sequential reaction pathway. An interpretation is impeded by the existence of several fragmentation pathways leading to these ion pairs. The broad $C^+ + S^+$ feature has a slope of around −2. For a sequential fragmentation via $HNC^+ + S^+$ a slope of −2.25 is predicted,[42] which is close enough to the value of −2 to suggest this pathway. Furthermore, for the isoelectronic OCS^{2+} molecule, a similar mechanism via $OC^+ + S^+$ was deduced from the $C^+ + S^+$ coincidence signal. Here, deviations between predicted and observed slopes were found to indicate that the secondary fragmentation takes place in the Coulomb field of the first ionic fragment.[43] The PIPICO maps also reveal ion pairs with a total charge of +3: $HNC^+ + S^{2+}$, $CN^+ + S^{2+}$ and -following S2p ionization-$HNC^{2+} + S^+$. They result from double Auger decay, e.g., from fragmentation of the triply charged $HNCS^{3+}$ that is observed in the TOF mass spectrum. The fragments of a two-body breakup, $HNC^+ + S^{2+}$ and $HNC^{2+} + S^+$, are associated with a slope of −2 in time-of-flight units, while $CN^+ + S^{2+}$ shows a shallower slope, as expected for a sequential loss of a neutral hydrogen atom.[44]

As in the mass spectrum, similar fragments are observed in the PIPICO maps following N1s, C1s, and S2p ionization of HNCS; however, with different relative intensities. The PIPICO maps prove the presence of NS^+ and CS^+ fragments, as well as HNC^+ and CN^+ in the respective overlapping signals in the mass spectra. Furthermore, an NH^+ fragment was identified unambiguously. Note that fragment ions produced in coincidence with H^+, for example, NCS^+, do not appear in our PIPICO maps but solely in the mass spectra because H^+ is not detected. Contamination by N_2 and HCN introduces the $N^+ + N^+$ pair (nitrogen 1s edge) as well as $CH^+ + N^+$ and $C^+ + N^+$ pairs (nitrogen and carbon 1s edge). Although the latter ion pair could, in principle, also be related to an HNCS fragmentation, it does not appear following S2p ionization (where no Auger decay of HCN is initiated), suggesting that $C^+ + N^+$ is mostly produced from HCN and not from HNCS.

In their study of HNCS double photoionization at 40.81 and 90 eV, Wallner et al. observed additional $H^+ + CS^+$ and $H^+ + S^+$ fragmentation channels[6] that cannot be detected by our setup but are likely present. They further observed CS^{2+} and recognized it to possibly include contributions from CO_2^{2+}. In our experiments, the occurrence of a CS^{2+} fragment (m/z 22) can be excluded on the basis of the mass spectrum in Figure 1. Moreover, a putative $SH^+ + CN^+$ ion pair, hidden by the more intense $HNC^+ + S^+$ ion signal, can be ruled out by its absence in our PIPICO maps.

To quantify the relative contributions of fragmentation channels following site-selective ionization, we evaluated their branching ratios. Further details on the determination of branching ratios are included in Section S3 in the SI. Table 1 summarizes the branching ratios of single ions and ion pairs obtained by integration from the mass spectra and PIPICO maps, respectively. The latter also allows elimination of contributions of N_2 and HCN.

The fragmentation of the C−S bond forming $HNC^+ + S^+$ shows the highest intensity at all three edges, with a slight preference after S2p ionization (38.5%) over C1s and N1s ionization (~35%). For an additional cleavage of the N−H bond, yielding $CN^+ + S^+$, a branching ratio of more than 20% is found at the N1s and C1s edges, while it is less abundant after

https://doi.org/10.1021/acs.jpca.6c00386
J. Phys. Chem. A 2026, 130, 2602−2611

Table 1. Branching Ratios After N1s, C1s, and S2p Electron Ionization of HNCS (in %)[a]

Ion (pair)	Nitrogen 1s	Carbon 1s	Sulfur 2p
$HNCS^{2+}$	4.5	1.7	18.2
NCS^{+}	1.2	<1	1.6
NCS^{2+}	1.4	1.7	1.4
$HNCS^{3+}$	–	–	<1
$NH^{+} + CS^{+}$	1.8	1.9	1.8
$N^{+} + CS^{+}$	1.6	1.5	1.3
$HNC^{+} + S^{+}$	34.7	34.5	38.5
$CN^{+} + S^{+}$	22.7	22.0	14.9
$HNC^{2+} + S^{+}$	–	–	1.2
$HNC^{+} + S^{2+}$	1.7	1.5	2.7
$CN^{+} + S^{2+}$	1.3	1.0	<1
$C^{+} + NS^{+}$	1.3	1.6	1.7
$NH^{+} + S^{+}$	1.8	2.7	1.4
$N^{+} + S^{+}$	8.3	9.3	3.9
$C^{+} + S^{+}$	17.7	19.8	10.4
Others	0.0	0.8	1.0

[a]Relative intensities were determined from PIPICO Maps (ion pairs) and mass spectra (single ions). Integrals of overlapping masses were derived from fitting with Gaussian functions. The branching ratios were normalized so that all channels sum up to 100% and corrected for isotopic patterns. Branching ratios <1% are not specified and are summarized in "others". Note that ion pairs including H^{+} cannot be deduced from this experiment's PIPICO Maps and are therefore not included in this table. The error of each branching ratio is estimated to be around ±15% of the respective branching ratio.

S2p ionization (15%). A similar effect is observed for the much less abundant ion pairs $HNC^{+} + S^{2+}$ and $CN^{+} + S^{2+}$. The most significant difference between the ionization sites is the preferred formation of the parent dication $HNCS^{2+}$ at the S2p edge, with a branching ratio of 18.2%, whereas its yield is below 5% at the N1s edge and even lower at the C1s edge. All these observations point toward a lower fragmentation tendency at the S2p edge in comparison to the N1s and C1s edges: at the S2p edge, bonds preferentially remain intact, while they show stronger and more similar fragmentation at the N1s and C1s edges. This trend is also reflected in the enhanced formation of atomic ion pairs ($C^{+} + S^{+}$, $N^{+} + S^{+}$) at the N1s and C1s edges compared to the S2p edge.

To investigate whether the fragmentation depends on the final state of the dication, the mass- and ion pair-selected Auger electron spectra were evaluated. They are shown in Figures 3 and 4 for the S2p and N1s edges, and Figure S4 in the SI for the C1s edge. The upper traces present the total Auger electron spectra measured in the present study in black. High-resolution reference spectra[7] obtained using a hemispherical analyzer are shown in red. Despite the lower resolution of the DTA, the absolute energies and relative intensities of the bands agree well. The Auger electron spectra of HNCS were discussed in ref 7, and therefore only a short summary is given here. The AES following S2p ionization (Figure 3a) is a superposition of the decay of the $S2p_{1/2}$ and $S2p_{3/2}$ core holes. At all three edges, the first region up to binding energies of 31 eV corresponds to $^{1}A'$ and $^{1}A''$ Auger final states with two holes in the HOMO (3a″) and HOMO−1 (12a′). The lowest dicationic triplet state $^{3}A''$ at 27.6 eV is only populated after S2p ionization and cannot be resolved here. Final states with the second hole in one of the deeper molecular orbitals (2a″ and 11a′) account for the second feature between 32−35 eV on the N1s and C1s edges. In contrast, states with the second

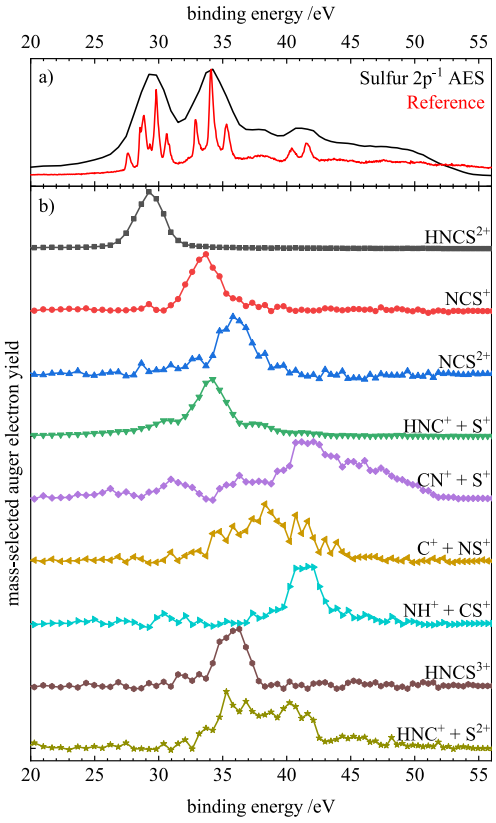

Figure 3. (a) The total Auger electron spectrum of HNCS at the S2p edge, shown in black, is compared with a higher-resolution reference spectrum in red. The latter was reproduced from ref 7 with permission from the PCCP Owner Societies. (b) Normalized mass- and ion pair-selected Auger electron spectra after S2p ionization of HNCS.

hole in the lower-lying 10a′ orbital (located at the sulfur atom) dominate this region following S2p ionization because of the small overlap of the 2a″ and 11a′ molecular orbitals with the S2p orbital. The most intense band is found between 35−40 eV in the N1s and C1s AES. Its lower intensity in the S2p AES is again due to the involvement of the molecular orbitals mainly located at the carbon and nitrogen atoms. In the region of a fourth band at the N1s edge (40−45 eV), the high-resolution $S2p^{-1}$ spectrum shows a double peak that appears only as a broader single feature in the present experiment. The double peak is due to two-hole final states with at least one hole in the sulfur-based 10a′ orbital.

Figures 3b and 4b present the mass- and ion pair-selected AES at the S2p and N1s edges. The upper traces show that the first band below 31 eV is nearly exclusively associated with $HNCS^{2+}$ formation at all edges. This first band shows a very high intensity in the total AES at the S2p edge, while its intensity is lower at the N1s edge and even lower at the C1s edge (compare Figure S4). This results from a different overlap of the respective core orbitals and valence orbitals involved in the Auger−Meitner decay of this band (HOMO and HOMO−1). Consequently, the yield of $HNCS^{2+}$ is significantly higher after $S2p^{-1}$ ionization. The formation of NCS^{+} ($+H^{+}$) sets in at $E_B = 31$ eV, coinciding with the second band in the S2p and N1s AES. This band has only very low intensity at the C1s edge; thus, nearly no NCS^{+} is observed following C1s ionization. The onset matches the previously determined experimental value of 31.2 ± 0.5 eV at $h\nu = 40.8$ eV and the calculated appearance energy (AE) of 30.90 eV.[6] NCS^{2+} is

https://doi.org/10.1021/acs.jpca.6c00386
J. Phys. Chem. A 2026, 130, 2602−2611

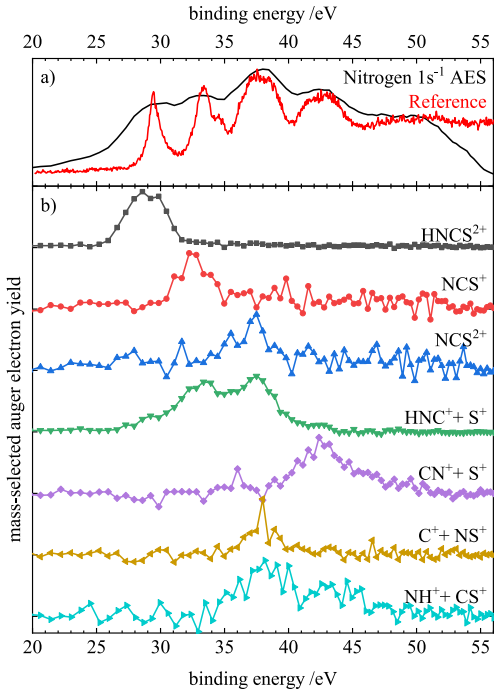

Figure 4. (a) The total Auger electron spectrum of HNCS at the N1s edge, shown in black, is compared to a higher-resolution reference spectrum in red. The latter was reproduced from ref 7 with permission from the PCCP Owner Societies. (b) Normalized mass- and ion pair-selected Auger electron spectra after N1s ionization of HNCS.

associated with Auger electrons of 34−40 eV binding energy both at the S2p and N1s edges. The N1s^{-1} Auger−Meitner decay in this region involves holes in the 2a″ and 11a′ orbitals (mainly located at N, C), while the S2p$_{3/2}^{-1}$ decay to ^{1}A″(10a′$^{-1}$3a″$^{-1}$) and ^{1}A′(10a′$^{-1}$12a′$^{-1}$) states dominates at the S2p edge. The onset of 34 eV matches the dissociation limit of 34.3 eV for HNCS^{2+} → NCS^{2+} ($^2\Sigma^+$) + H calculated by Wallner et al. and their experimental onset of 35.0 ± 0.4 eV.[6]

The formation of the ion pair HNC$^+$ + S$^+$, which is the dominant product channel at all three edges, sets in at the high-energy side of the first band in the AES at around 29 eV. This is consistent with a calculated appearance energy of 29.26 eV and an experimental onset at 29.1 ± 0.2 eV.[6] Based on our data, a rearrangement to HCN$^+$ cannot be excluded. The channel CN$^+$ + S$^+$ appears at higher binding energies compared to HNC$^+$ + S$^+$, as it requires additional N−H bond cleavage. It sets in at around 38 eV at all three edges. The comparatively low population of final states with binding energies >36 eV in the S2p^{-1} AES results in a lower branching ratio of CN$^+$ + S$^+$ after S2p ionization than after N1s and C1s ionization. The ion pair-selected AES of C$^+$ + NS$^+$ shows a maximum at 38 eV at all three edges. This could imply the population of an Auger final state that selectively leads to a rearrangement required for N−S bond formation. In particular, the N1s and C1s edges reveal relatively sharp signals, while a broader energy range is covered at the S2p edge. For the ion pair NH$^+$ + CS$^+$, which is similarly weak in the PIPICO map, the signal-to-noise ratio in the ion pair-selected AES at the N1s edge is very low. The spectrum at the S2p edge, however, shows that this ion pair is formed after the decay to ^{1}A′(10a′$^{-2}$) and ^{1}A′(9a′$^{-1}$10a′$^{-1}$) final states, which are responsible for the double peak structure around 41 eV visible in the total AES (Figure 3a).

At all three edges, the fragments HNC$^+$ + S$^+$, CN$^+$ + S$^+$, NCS$^+$ + H$^+$ and NCS^{2+} appear at similar binding energies, respectively, although different Auger final states are populated at the different edges. This demonstrates that either different electronic states show similar fragmentation dynamics, or fragmentation is preceded by deactivation to a lower dicationic state, essentially following an ergodic mechanism and governed by the total amount of internal energy available for the dissociation. The high branching ratio of HNC$^+$ + S$^+$ (∼35%) results from it being the lowest-energy fragmentation channel. Furthermore, different relative populations of final states in the total AES at the different edges can qualitatively explain the differences in branching ratios. For example, the higher branching ratio of HNCS^{2+} following S2p^{-1} ionization is a consequence of the higher contribution of low-binding energy final states in the S2p^{-1} AES. The stronger fragmentation tendency observed at the C1s and N1s edges is rationalized by the stronger contribution of high-binding energy final states to the N1s^{-1} and C1s^{-1} AES. This results in a higher branching ratio of strongly fragmented ion pairs like CN$^+$ + S$^+$ and atomic fragments following N1s^{-1} and C1s^{-1} ionization.

Mass- and ion pair-selected spectra for triply charged species were extracted at the S2p edge. Note that triple ionization energies or onsets for dissociation cannot be deduced from these spectra because the information on the kinetic energy of the second Auger electron is lost by our single-start-multiple-stop coincidence scheme. However, the spectra (see Figure 3b) reveal that HNCS^{3+} is formed by Auger−Meitner processes contributing to the 34−38 eV region of the AES, while the breakup to HNC$^+$ + S^{2+} extends up to 43 eV.

Resonant Auger-Meitner Processes

In resonant Auger−Meitner processes, a neutral core-excited state decays and ejects an Auger electron to yield a singly ionized species. The Auger final state can be either a one-hole (1h, participator decay) or a two-hole-one-particle (2h1p, spectator decay) electronic configuration. The fragmentation following core excitation and resonant Auger−Meitner decay was also studied after excitation into the LUMO (13a′) and LUMO+1 (4a″) at all three edges. The positions of the excited states and the resonant Auger electron spectra were reported in our previous study.[7]

Figure 5 depicts the TOF mass spectra after resonant excitation of nitrogen and carbon 1s electrons into the LUMO +1 (4a″). In addition, the spectrum after S2p excitation is shown, which is a superposition of the excitations S2p$_{3/2}$→ 4a″ (LUMO+1) and S2p$_{1/2}$→ 13a′ (LUMO) with an approximate relative intensity of 2:1.[7] The mass spectra following 13a′ (LUMO) excitation are shown in Figure S5 in the SI. All spectra were corrected for the contributions from direct valence photoionization. Photoelectrons appear in the same kinetic energy range as the Auger electrons, and ionic fragments from these processes are therefore detected in our mass spectra. Since the sulfur 2p edge (∼165 eV) lies closest in energy to the valence ionization region, the effect on the spectrum is strongest following the excitation of sulfur 2p electrons. As a correction, off-resonant spectra at photon energies a few electronvolts below the first resonance were recorded at all edges and subtracted from the respective mass spectra. Their scaling factor was determined from the purely off-resonant mass signal of water (m/z 18) in both the off-

https://doi.org/10.1021/acs.jpca.6c00386
J. Phys. Chem. A 2026, 130, 2602−2611

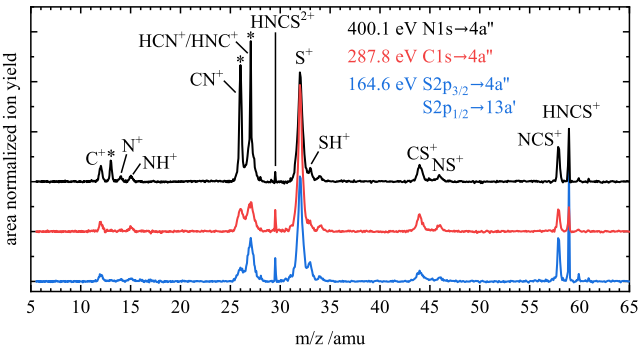

Figure 5. TOF mass spectrum after resonant excitation of N1s, C1s, and $S2p_{3/2}$ electrons into the 4a″ orbital (LUMO+1) of HNCS. The spectrum after S2p excitation is a superposition of $S2p_{3/2} \rightarrow 4a''$ and $S2p_{1/2} \rightarrow 13a'$ excitation. Asterisks indicate ions that originate (partially) from the resonant excitation of an HCN impurity.

resonant and resonant spectra. In Figure S6 in the SI, we show an example of this correction at the S2p edge. In the mass spectra in Figure 5, a narrow signal for the parent ion $HNCS^+$ is visible at m/z 59, which shows the highest intensity after S2p excitation. Fragment ions show broader features because of the kinetic energy released in the dissociation. As expected, the width of the signals is smaller than that for the dissociation of dications. The products of an N−H and N−C bond cleavage, NCS^+ and CS^+, are found at m/z 58 and 44, respectively. Smaller, however clearly discernible signals of NS^+ and SH^+ are a sign of an isomerization in the cation, as we can rule out the presence of other isomers based on the NEXAFS spectra. An intense broad S^+ signal is observed at all edges, while the parent dication appears at m/z 29.5. Further fragments are HNC^+/HCN^+, CN^+, NH^+, N^+ and C^+. Upon N1s excitation, narrow signals at m/z 27, 26, and 13 (HCN^+, CN^+, CH^+) result from the excitation of an HCN impurity in the sample that was absent at the other edges. HCN^+ and CN^+ overlap with fragment ions from HNCS. As the latter appear as broader features surrounding the peak, the two components were separated by fitting with two Gaussian functions. Table 2 gives the branching ratios (corrected for HCN impurities) after resonant excitation of N1s, C1s, and S2p electrons into the LUMO and LUMO+1.

Here, we will concentrate on the excitation into the 4a″ orbital (LUMO+1). S^+ shows the highest branching ratio at all three edges, in particular, upon C1s excitation (50.8% compared to 42.1% and 40.5% upon N1s and S2p excitation). The second most abundant fragment, HNC^+, is significantly less pronounced, with a branching ratio below 20%. CN^+ is formed with a yield of around 10% upon N1s and C1s excitation, while it is less intense after S2p excitation, as can be seen from the mass spectrum in Figure 5. On the other hand, S2p excitation shows a propensity for the formation of $HNCS^+$, NCS^+, and SH^+ compared to C1s and N1s excitation. Similar trends are observed upon site-selective excitation into the 13a′ orbital.

To rationalize differences in the fragmentation pattern upon resonant excitation at different atomic sites, mass-selected resonant Auger electron spectra (ms-RAES) were evaluated. Figure 6a shows the total RAES upon C1s→4a″ excitation recorded in the present work (black) with a higher-resolution reference spectrum[7] (red) for comparison. The ms-RAES were obtained by selecting only Auger electrons detected in coincidence with an ionic fragment, as depicted in Figure 6b. Other ms-RAES recorded for 13a′ and 4a″ excitation at the N1s, C1s, and S2p edges are given in Section S6 in the SI. A previous analysis of the C1s RAES in Figure 6a assigned the features at around 10.0 eV, 13.5 eV, 15.2 eV, and 18.2 eV to 1 h participator final states with a hole in the 3a″/12a′, 2a′′/11a′, 10a′ and 9a′ orbitals. 2h1p spectator final states with $12a'^{-1}3a''^{-1}4a''^{1}$ occupations were found to set in at around 16 eV.[7] Although the resolution is significantly lower, the main features of the reference spectrum are reproduced sufficiently well. In particular, the participator states at 13.5 eV are resonantly enhanced upon C1s excitation, as is the decay to final states with binding energies >18 eV.[7] The ms-RAES in Figure 6b shows that the cationic ground state at 10.0 eV is

Table 2. Branching Ratios After Resonant Excitation of N1s, C1s, and S2p Electrons into 13a′ (LUMO) and 4a″ (LUMO+1) Orbitals of HNCS (in %)[a]

		13a′ (LUMO) excitation			4a″ (LUMO+1) excitation		
ion	m/z	Nitrogen 1s	Carbon 1s	Sulfur $2p_{3/2}$	Nitrogen 1s	Carbon 1s	Sulfur $2p_{3/2}$
$HNCS^+$	59	2.2	3.0	10.7	4.2	2.2	8.1
NCS^+	58	6.2	4.9	9.0	6.8	5.1	9.3
NS^+	46	2.3	1.5	1.2	1.9	2.1	1.5
CS^+	44	7.1	7.0	5.2	6.6	7.4	5.2
SH^+	33	5.1	4.1	7.0	3.3	3.6	7.1
S^+	32	43.5	47.3	41.3	42.1	50.8	40.5
HNC^{+b}	27	19.0	14.1	15.8	19.7	14.4	18.1
CN^{+b}	26	9.2	10.8	4.7	9.2	9.1	5.6
NH^+	15	1.1	1.2	1.0	1.3	1.3	0.9
N^{+c}	14	1.0	1.2	0.7	1.1	0.5	0.5
C^{+c}	12	3.0	4.0	2.0	3.4	2.2	1.9
$HNCS^{2+}$	29.5	0.3	0.9	1.4	0.4	1.3	1.3

[a]Relative intensities were determined from the mass spectra in Figures 5 and S5. Integrals of overlapping masses were derived from fitting with Gaussian functions. The branching ratios were normalized so that all channels sum up to 100% and corrected for isotopic patterns. The absolute error of each branching ratio is estimated to be around ±0.5%. Note that the branching ratios following $S2p_{3/2}$ excitation into the 4a″ orbital are a superposition of the $S2p_{3/2} \rightarrow 4a''$ and $S2p_{1/2} \rightarrow 13a'$ excitation. [b]Contributions originating from an HCN impurity were subtracted, and only the fraction assigned to HNCS fragmentation is given. [c]Branching ratios of C^+ and N^+ are likely to be contaminated by HCN for the N1s→13a′/4a″ and C1s→13a′ excitation.

https://doi.org/10.1021/acs.jpca.6c00386
J. Phys. Chem. A 2026, 130, 2602−2611

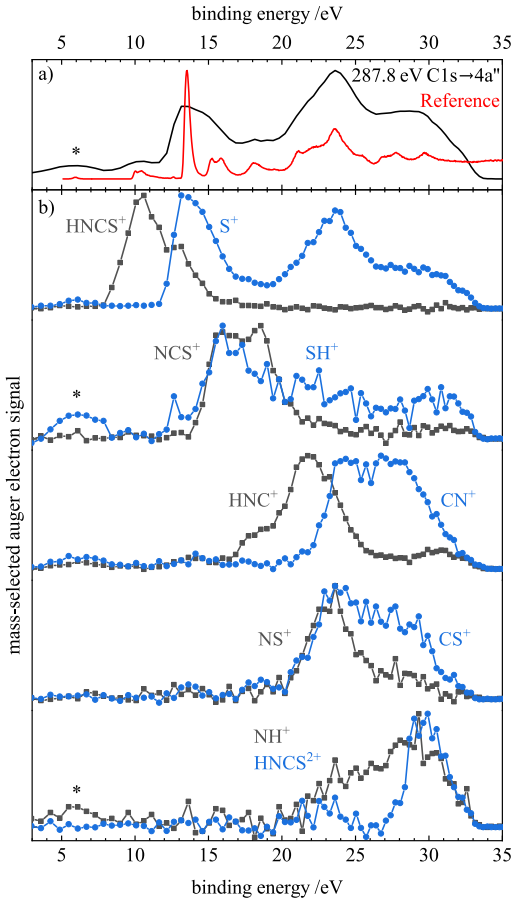

Figure 6. (a) The total resonant Auger electron spectrum upon C1s→4a″ excitation of HNCS, shown in black, is compared to a higher-resolution reference spectrum. The latter was reproduced from ref 7 with permission from the PCCP Owner Societies. (b) Normalized mass-selected resonant Auger electron spectra. The asterisks mark signals that result from carbon 1s ionization by second-harmonic light.

associated purely with $HNCS^+$ formation. The resonant Auger–Meitner decay to $\tilde{A}^+\,^2A''(2a''^{-1})$ and $\tilde{B}^+\,^2A'(11a'^{-1})$ final states at ∼13.5 eV leads to S^+ fragments. A recent investigation of dissociative photoionization found an AE_{0K} of 13.22 ± 0.02 eV for S^+ + HCN formation, while S^+ + HNC is formed at higher binding energies.[5] Within the resolution of the present experiment, the AE coincides with the onset in the ms-RAES of S^+ in Figure 6b. S^+ is formed up to binding energies >30 eV, presumably in coincidence with varying neutral fragments. The formation of NCS^+ and SH^+ sets in simultaneously at around 15 eV, where the $^2A'(10a'^{-1})$ state and low-energy spectator states are populated, also in agreement with valence photoionization.[5] The second maximum at ∼18 eV in the ms-RAES of NCS^+ reveals that this ion is also formed by the decay to the $^2A'(9a'^{-1})$ state. The continuous signal of SH^+ (m/z 33) at higher binding energies is artificial and results from a broadening of the neighboring S^+ band in the mass spectrum. The $^2A'(9a'^{-1})$ state around 18 eV also leads to HNC^+/HCN^+ formation. Its ms-RAES confirms that the sample is free of an HCN impurity, as no signal is observed at the ionization energy of HCN (13.60 eV[45]) and its onset matches the previously determined one for HNCS→HNC^+/HCN^+ + S (17.5 ± 0.5 eV[5]). The decaying HNC^+/HCN^+ signal matches the rise of the CN^+ signal, suggesting that HNC^+/HCN^+ is not stable at higher binding energies and further N–H fragmentation yields CN^+, which sets in at around 22–23 eV, matching the calculated dissociation limit of 22.11 eV. This is lower than the previously determined experimental onset of 24.6 ± 0.5 eV that might suffer from a low signal in the corresponding spectrum.[5] NS^+ and CS^+ formations set in simultaneously above 20 eV. The latter ion seems to be more stable at higher binding energies. Their maximum at around 23 eV coincides with the population of spectator final states with at least one hole in the 2a″ or 9a′ orbital.[7] Both CS^+ and NH^+ result from simple N–C bond cleavage. Although these ions were (nearly) not observed in the PEPICO experiments[5] (likely due to their low intensity), they appear clearly in our mass spectrum and in the ms-RAES above 20 eV. The dication $HNCS^{2+}$ shows a sharp rise at around 28 eV, in agreement with the double ionization energy of 27.6 eV.[7]

The ms-RAES upon 4a″ excitation of the N1s and S2p electrons (see Figures S7 and S8 in the SI) show similar fragmentation onsets to the C1s edge. Differences are found only for the CN^+ fragment, which shows a lower onset due to the fragmentation of an HCN contamination, and for the NS^+ and CS^+ fragments, which rise more slowly and at lower binding energies at the S2p edge.

Although the fragmentation onsets are similar, the intensities in ms-RAES are distributed differently at the three edges because the transition strengths into the Auger final states are different. The population of the Auger final states is determined by the overlap between the core orbital and the valence orbitals involved in the Auger–Meitner decay. The increased yield of S^+ at the C1s edge compared to the other edges can be understood from its ms-RAES: S^+ is the only ionic fragment that is formed from the $\tilde{A}^+\,^2A''(2a''^{-1})$ and $\tilde{B}^+\,^2A'(11a'^{-1})$ final states. The corresponding band at 13.5 eV in the RAES is resonantly enhanced after C1s excitation (for 4a″ even more than for 13a′ excitation) because of the high overlap between the C1s orbital and the 2a′′ or 11a′ valence orbital, leading to a stronger S^+ formation following C1s excitation. After N1s and S2p electron excitation, no enhancement of the band at 13.5 eV is observed in the RAES. Furthermore, C1s and N1s excitations lead to a stronger enhancement of the spectator final states with binding energies >20 eV compared to S2p excitation. Therefore, CN^+, which is formed in this binding energy region (>20 eV), shows a much higher branching ratio after C1s and N1s excitation. On the other hand, S2p excitation leads to high decay rates for the participator states at ∼10 and 15 eV, with $3a''^{-1}/12a'^{-1}$ and $10a'^{-1}$ occupation, respectively. This is because these orbitals show significant density at the sulfur atom. Since the Auger–Meitner decay to the cationic ground state at 10.0 eV solely induces $HNCS^+$ formation, the $HNCS^+$ yield upon S2p excitation is higher compared to C1s and N1s excitation. Similarly, the resonant enhancement of the $^2A'(10a'^{-1})$ state at ∼15 eV is responsible for the higher branching ratios of NCS^+ and SH^+ fragments, which were found to be associated with the population of this state.

DISCUSSION

For both core ionization and excitation of HNCS, the (fragment) branching ratios are found to moderately depend on the initially ionized or excited atomic site. Here, we want to compare the fragmentation of HNCS after normal Auger–Meitner decay with the well-studied isovalent molecule

https://doi.org/10.1021/acs.jpca.6c00386
J. Phys. Chem. A 2026, 130, 2602–2611

isocyanic acid, HNCO. In doing so, we compare molecules of similar connectivity but different nuclear charge, since the terminal sulfur atom is substituted by an oxygen atom. A previous comparison of the normal Auger electron spectra of the two molecules revealed similar final state occupations.[7] However, different energies of the oxygen 2p and sulfur 3p valence orbitals were found to result in a higher population of high-binding-energy final states in the $O1s^{-1}$ AES of HNCO compared to the $S2p^{-1}$ AES of HNCS.[7] The fragmentation of doubly charged HNCO was also studied by coincidence spectroscopy after Auger−Meitner decay at the N1s and O1s edges[32] and after photoionization at 100 eV.[46]

Due to their similar connectivity, one could expect similar fragmentation patterns for isothiocyanic acid and isocyanic acid. Indeed, we observe mostly similar (fragment) ions following Auger−Meitner decay. For example, in both cases, the parent dication is stable, and NCS^{2+}/NCO^{2+} is detected, which is not the case for the HNCO isomer, fulminic acid, HCNO.[34] However, the branching ratios of the (fragment) ions exhibit significant differences between HNCS and HNCO. Upon the ionization of HNCO by O1 s^{-1} and N1 s^{-1} all ion pairs from a two-body fragmentation - $H^+ + NCO^+$, $NH^+ + CO^+$, and $HNC^+ + O^+$ - as well as the products of an additional N−H bond fission, $N^+ + CO^+$ and $CN^+ + O^+$, were found to be produced in high abundance. While the branching ratio of $H^+ + NCO^+$ is similar at both edges (∼16%), O1 s^{-1} ionization enhances $NH^+ + CO^+$ and $HNC^+ + O^+$ compared to N1 s^{-1} ionization, which leads preferentially to the formation of $N^+ + CO^+$ and $CN^+ + O^+$.[32]

These results are in contrast to the present observations for HNCS, where the C−S bond dissociation to $HNC^+ + S^+$ is by far the strongest ion pair dissociation channel at all edges (∼35%). The ion pairs resulting from an N−H and N−C bond cleavage ($H^+ + NCS^+$, $NH^+ + CS^+$) are observed with branching ratios <2%, much lower than for HNCO. The parent dication, which is formed with a yield of 18.2% at the sulfur edge in HNCS, is less abundant in HNCO (<3%).[32]

The higher yield of $H^+ + NCO^+$ compared to $H^+ + NCS^+$ results from it being the only open fragmentation channel in $HNCO^{2+}$ until the barriers for N−C and C−O bond dissociation are passed. Compared with $HNCO^{2+}$, the N−H bond fragmentation in $HNCS^{2+}$ (to $H^+ + NCS^+$) is associated with a higher barrier. Instead, $HNCS^{2+} \rightarrow HNC^+ + S^+$ represents the lowest fragmentation channel, resulting in a lower branching ratio for $H^+ + NCS^+$, while $HNC^+ + S^+$ is the major fragmentation pathway following Auger−Meitner decay of HNCS. The lower $HNCO^{2+}$ ion yield does not result from a lower dissociation barrier in the dication, as the lowest fragmentation channel in HNCO and HNCS was found to open at around 1.5 eV above their respective double ionization energy.[6,32] We therefore assume a slower dissociation of $HNCS^{2+}$ to $HNC^+ + S^+$ slightly above the dissociation threshold.

Interestingly, we detect the metastable $HNCS^{3+}$ trication after $S2p^{-1}$ ionization, whereas $HNCO^{3+}$ was not observed.[32,46,47] While $HNCO^{3+}$ was found to fragment mostly into three singly charged ions,[47] we clearly observe the fragmentation of $HNCS^{3+}$ into ion pairs (one singly and one doubly charged cation) at all edges after the Auger−Meitner decay (see Figure 2).

For both HNCS and HNCO, fragments were found that result from an isomerization of the ion. Upon normal Auger−Meitner decay of HNCO, an isomerization on the cationic surface was found to yield $H^+ + NO^+ + C$. The newly formed N−O bond was explained by dissociation into $H^+ + NCO^+$ followed by an N-migration in NCO^+ via a three-membered ring transition state and subsequent fragmentation.[32] Similar to NO^+, we detect NS^+ upon core ionization of HNCS. Here, NS^+ appears in coincidence with C^+ rather than H^+. Therefore, we can rule out a pathway similar to the one in HNCO that would occur via a rearrangement of NCS^+.

CONCLUSION

The fragmentation of isothiocyanic acid following core ionization and excitation was investigated by Auger electron−ion coincidence spectroscopy at the N1s, C1s, and S2p edges.

After core ionization, the majority of dications fragment by a C−S bond cleavage with initial charge separation, yielding $HNC^+ + S^+$ and $CN^+ + S^+$. Nevertheless, fragmentation patterns were found to differ depending on the initially core-ionized atom: while $N1s^{-1}$ and $C1s^{-1}$ ionizations exhibit an enhanced and more similar fragmentation tendency, $S2p^{-1}$ ionization favors the intact parent dication $HNCS^{2+}$. The trication $HNCS^{3+}$, that is produced by double Auger decay, was observed only at the S2p edge, while ion pairs from its dissociation appeared at all edges. The ion pair $C^+ + NS^+$ results from a rearrangement and was found with a yield <2%.

Resonant core excitation predominantly yields S^+ and HNC^+ fragments. As in previous experiments[48] on singly ionized HNCS, we observed the rearranged fragments SH^+ and NS^+. When comparing the fragmentation following excitation into 13a′ (LUMO) and 4a″ (LUMO+1), mostly similar trends were observed. S2p electron excitation was found to enhance $HNCS^+$, NCS^+ and SH^+ formation, whereas N1s and C1s electron excitations prefer CN^+ formation.

Mass- and ion pair-selective (resonant) Auger electron spectra revealed only minor differences in the fragmentation onsets at the N1s, C1s, and S2p edges. These onsets agree mostly with appearance energies from recent valence-shell ionization studies.[5,6] We were able to explain the main differences in the fragmentation of core-excited/ionized HNCS by the different population of Auger final states at the N1s, C1s, and S2p edges. As the Auger decay rate depends on the overlap between the respective core hole and valence orbitals, the relative population of the final states in the Auger electron spectra is site-specific, resulting in different fragmentation patterns. This is in agreement with findings from previous studies.[24,29] Furthermore, HNCS was compared with its oxygen congener, isocyanic acid, HNCO, and differences in the fragmentation following core ionization were rationalized by the different energetic ordering of the fragmentation onsets.

This study extends the knowledge of the fragmentation of the astrochemical molecule isothiocyanic acid into the soft X-ray region. Given the presence of X-ray emitters in space, this information could be useful for astrochemical models.

ASSOCIATED CONTENT

Supporting Information

The Supporting Information is available free of charge at https://pubs.acs.org/doi/10.1021/acs.jpca.6c00386.

See Supporting Information for time-of-flight mass and NEXAFS spectra of HNCS, mass- and ion pair-selected Auger electron spectra, a detailed description of the

https://doi.org/10.1021/acs.jpca.6c00386
J. Phys. Chem. A 2026, 130, 2602−2611

treatment of false coincidences, and the determination of branching ratios (PDF)

AUTHOR INFORMATION

Corresponding Author

Ingo Fischer − *Institute of Physical and Theoretical Chemistry, University of Würzburg, Würzburg D-97074, Germany;* orcid.org/0000-0001-8978-4013; Phone: +49 931 31 86360; Email: ingo.fischer@uni-wuerzburg.de

Authors

Dorothee Schaffner − *Institute of Physical and Theoretical Chemistry, University of Würzburg, Würzburg D-97074, Germany;* orcid.org/0009-0003-6572-9214

Lilith Wohlfart − *Institute of Physical and Theoretical Chemistry, University of Würzburg, Würzburg D-97074, Germany*

Katharina Theil − *Institute of Physical and Theoretical Chemistry, University of Würzburg, Würzburg D-97074, Germany*

Emil Karaev − *Institute of Physical and Theoretical Chemistry, University of Würzburg, Würzburg D-97074, Germany*

John D. Bozek − *Synchrotron SOLEIL, Saint-Aubin 91190, France;* orcid.org/0000-0001-7486-7238

Complete contact information is available at: https://pubs.acs.org/10.1021/acs.jpca.6c00386

Author Contributions

D.S.: formal analysis (lead); investigation (lead); and writing—original draft (lead). L.W.: investigation (equal). K.T.: investigation (equal). E.K.: investigation (equal). J.B.: investigation (equal). I.F.: conceptualization (lead); funding acquisition (lead); investigation (equal); supervision (lead); and writing—review and editing (equal).

Notes

The authors declare no competing financial interest.

ACKNOWLEDGMENTS

The work was funded by the Deutsche Forschungsgemeinschaft, Contract No. FI575/19-1, and performed on the PLEIADES beamline under Proposal No. 20231297. We acknowledge SOLEIL for provision of synchrotron radiation facilities and thank the PLEIADES beamline team for their assistance. D.S. acknowledges a Kekulé fellowship from the Fonds der Chemischen Industrie (FCI), LW acknowledges a fellowship from the Rosa Luxemburg foundation.

REFERENCES

(1) Miron, C.; Morin, P.; Quack, M.; Merkt, F. *Handbook of High-resolution Spectroscopy*; Wiley, 2011.

(2) Frerking, M. A.; Linke, R. A.; Thaddeus, P. Interstellar isothiocyanic acid. *Astrophys. J.* **1979**, *234*, L143−L145.

(3) Adande, G. R.; Halfen, D. T.; Ziurys, L. M.; Quan, D.; Herbst, E. Observations of the [HNCS]/[HSCN] ratio in Sgr B2 and TMC-1: Evidence for low-temperature gas-phase chemistry. *Astrophys. J.* **2010**, *725*, 561−570.

(4) Schaffner, D.; Bellili, A.; Gerlach, M.; Karaev, E.; Mogren Al Mogren, M.; Bozek, J.; Fischer, I.; Hochlaf, M. Photoelectron spectrum of isothiocyanic acid, HNCS: Theory and experiment. *J. Chem. Phys.* **2025**, *162*, 164310.

(5) Olsson, E.; Schaffner, D.; Bellili, A.; Wallner, M.; Daver Ideböhn, V.; Squibb, R. J.; Parriani, M.; Gerlach, M.; Hemberger, P.; Lundberg, S.; et al. State-selective fragmentation of singly ionized HNCS: Experiment and theory. *J. Chem. Phys.* **2025**, *163* (20), 204303.

(6) Wallner, M.; Olsson, E.; Ideböhn, V.; Parriani, M.; Squibb, R. J.; Lundberg, S.; Cole, D.; Falcinelli, S.; Stranges, S.; Brunetti, B.; et al. Structure and fragmentation of doubly ionized HNCS. *J. Chem. Phys.* **2024**, *161* (4), 044313.

(7) Schaffner, D.; Gerlach, M.; Karaev, E.; Bozek, J.; Fischer, I.; Fink, R. F. Experimental and theoretical investigation of the Auger electron spectra of isothiocyanic acid, HNCS. *Phys. Chem. Chem. Phys.* **2024**, *26*, 27972−27987.

(8) Feigelson, E. D.; Montmerle, T. High-Energy Processes in Young Stellar Objects. *Annu. Rev. Astron. Astrophys.* **1999**, *37*, 363−408.

(9) Kastner, J. H.; Balick, B.; Blackman, E. G.; Frank, A.; Soker, N.; Vrtlek, S. D.; Li, J. A Compact X-Ray Source and Possible X-Ray Jets within the Planetary Nebula Menzel 3. *Astrophys. J.* **2003**, *591* (1), L37.

(10) Ankerhold, U.; Esser, B.; von Busch, F. Ionization and fragmentation of OCS and CS_2 after photoexcitation around the sulfur 2p edge. *Chem. Phys.* **1997**, *220*, 393−407.

(11) Erman, P.; Karawajczyk, A.; Rachlew, E.; Stankiewicz, M.; Franzén, K. Y. State selective photon induced formation of triply charged fragments from the core excited OCS molecule. *J. Chem. Phys.* **1997**, *107* (24), 10827−10828.

(12) Kaneyasu, T.; Ito, M.; Hikosaka, Y.; Shigemasa, E. Stability and Fragmentation of OCS^{2+} Studied by Using Auger-Electron-Ion Coincidence Measurement. *J. Korean Phy. Soc.* **2009**, *54* (9(5)), 371−375.

(13) Hayes, R. G.; Eberhardt, W. Electron-ion and ion-ion studies of the behavior of CS_2 upon core electron excitation. *J. Chem. Phys.* **1991**, *94*, 6398−6405.

(14) Hatherly, P. A.; Codling, K.; Stankiewicz, M.; Roper, M. Near-threshold site-selected dissociative ionization of core-excited carbon dioxide. *J. Phys. B: at., Mol. Opt. Phys.* **1995**, *28*, 3249.

(15) Eland, J. H. D.; Zagorodskikh, S.; Squibb, R. J.; Mucke, M.; Sorensen, S. L.; Feifel, R. Carbon dioxide ion dissociations after inner shell excitation and ionization: The origin of site-specific effects. *J. Chem. Phys.* **2014**, *140*, 184305.

(16) Eberhardt, W.; Sham, T. K.; Carr, R.; Krummacher, S.; Strongin, M.; Weng, S. L.; Wesner, D. Site-Specific Fragmentation of Small Molecules Following Soft-X-Ray Excitation. *Phys. Rev. Lett.* **1983**, *50*, 1038−1041.

(17) Wieland, H.; Hermann, B.; Klaus, M.-D.; Schlag, E. W. Selective fragmentation of nitrous oxide by site-specific N (1s) excitation using soft X-ray synchrotron radiation. *Phys. Scr.* **1990**, *41* (6), 814.

(18) Morin, P.; Simon, M.; Miron, C.; Leclercq, N.; Hansen, D. L. Electron-ion spectroscopy: a probe of molecular dynamics. *J. Electron Spectrosc. Relat. Phenom.* **1998**, *93*, 49−60.

(19) Mocellin, A.; Wiesner, K.; Sorensen, S. L.; Miron, C.; Le Guen, K.; Céolin, D.; Simon, M.; Morin, P.; Machado, A. B.; Björneholm, O.; et al. Site selective dissociation upon core ionization of ozone. *Chem. Phys. Lett.* **2007**, *435* (4−6), 214−218.

(20) Salén, P.; Kamińska, M.; Squibb, R. J.; Richter, R.; Alagia, M.; Stranges, S.; van der Meulen, P.; Eland, J. H. D.; Feifel, R.; Zhaunerchyk, V. Selectivity in fragmentation of N-methylacetamide after resonant K-shell excitation. *Phys. Chem. Chem. Phys.* **2014**, *16*, 15231−15240.

(21) Lin, Y. S.; Tsai, C. C.; Lin, H. R.; Hsieh, T. L.; Chen, J. L.; Hu, W. P.; Ni, C. K.; Liu, C. L. Highly Selective Dissociation of a Peptide Bond Following Excitation of Core Electrons. *J. Phys. Chem. A* **2015**, *119*, 6195−6202.

(22) Habenicht, W.; Baiter, H.; Mueller-Dethlefs, K.; Schlag, E. W. Memory effects in molecular fragmentation induced by site-specific core excitation using a reflection time-of-flight mass spectrometer. *J. Phys. Chem.* **1991**, *95*, 6774−6780.

(23) Liu, X. J.; Prümper, G.; Kukk, E.; Sankari, R.; Hoshino, M.; Makochekanwa, C.; Kitajima, M.; Tanaka, H.; Yoshida, H.; Tamenori, Y.; et al. Site-selective ion production of the core-excited CH_3F

molecule probed by Auger-electron−ion coincidence measurements. *Phys. Rev. A* **2005**, *72* (4), 042704.
(24) Bolognesi, P.; Kettunen, J. A.; Cartoni, A.; Richter, R.; Tosic, S.; Maclot, S.; Rousseau, P.; Delaunay, R.; Avaldi, L. Site- and state-selected photofragmentation of 2Br-pyrimidine. *Phys. Chem. Chem. Phys.* **2015**, *17*, 24063−24069.
(25) Miron, C.; Simon, M.; Leclercq, N.; Hansen, D. L.; Morin, P. Site-Selective Photochemistry of Core Excited Molecules: Role of the Internal Energy. *Phys. Rev. Lett.* **1998**, *81*, 4104−4107.
(26) Le Guen, K.; Ahmad, M.; Céolin, D.; Lablanquie, P.; Miron, C.; Penent, F.; Morin, P.; Simon, M. Influence of formation path on the CH_2BrCl^{2+} dissociation dynamics. *J. Chem. Phys.* **2005**, *123*, 084302.
(27) Kukk, E.; Ha, D. T.; Wang, Y.; Piekarski, D. G.; Diaz-Tendero, S.; Kooser, K.; Itälä, E.; Levola, H.; Alcamí, M.; Rachlew, E.; Martín, F. Internal energy dependence in x-ray-induced molecular fragmentation: An experimental and theoretical study of thiophene. *Phys. Rev. A* **2015**, *91*, 043417.
(28) Sen, S.; Mandal, S.; Sen, A.; Gopal, R.; Ben Ltaief, L.; Turchini, S.; Catone, D.; Zema, N.; Coreno, M.; Richter, R.; Mudrich, M.; Krishnan, S. R.; Sharma, V. Fragmentation dynamics of doubly charged camphor molecule following C 1s Auger decay. *Phys. Chem. Chem. Phys.* **2022**, *24*, 2944−2957.
(29) Levola, H.; Itälä, E.; Schlesier, K.; Kooser, K.; Laine, S.; Laksman, J.; Ha, D. T.; Rachlew, E.; Tarkanovskaja, M.; Tanzer, K.; Kukk, E. Ionization-site effects on the photofragmentation of chloro- and bromoacetic acid molecules. *Phys. Rev. A* **2015**, *92*, 063409.
(30) Inhester, L.; Oostenrijk, B.; Patanen, M.; Kokkonen, E.; Southworth, S. H.; Bostedt, C.; Travnikova, O.; Marchenko, T.; Son, S. K.; Santra, R.; Simon, M.; Young, L.; Sorensen, S. L. Chemical Understanding of the Limited Site-Specificity in Molecular Inner-Shell Photofragmentation. *J. Phys. Chem. Lett.* **2018**, *9*, 1156−1163.
(31) Holzmeier, F.; Wolf, T. J. A.; Gienger, C.; Wagner, I.; Bozek, J.; Nandi, S.; Nicolas, C.; Fischer, I.; Gühr, M.; Fink, R. F. Normal and resonant Auger spectroscopy of isocyanic acid, HNCO. *J. Chem. Phys.* **2018**, *149*, 034308.
(32) Gerlach, M.; Fantuzzi, F.; Wohlfart, L.; Kopp, K.; Engels, B.; Bozek, J.; Nicolas, C.; Mayer, D.; Gühr, M.; Holzmeier, F.; et al. Fragmentation of isocyanic acid, HNCO, following core excitation and ionization. *J. Chem. Phys.* **2021**, *154*, 114302.
(33) Gerlach, M.; Preitschopf, T.; Karaev, E.; Quitián-Lara, H. M.; Mayer, D.; Bozek, J.; Fischer, I.; Fink, R. F. Auger electron spectroscopy of fulminic acid, HCNO: an experimental and theoretical study. *Phys. Chem. Chem. Phys.* **2022**, *24*, 15217−15229.
(34) Gerlach, M.; Schaffner, D.; Preitschopf, T.; Karaev, E.; Bozek, J.; Holzmeier, F.; Fischer, I. X-ray induced fragmentation of fulminic acid, HCNO. *J. Chem. Phys.* **2023**, *159*, 114306.
(35) Céolin, D.; Miron, C.; Simon, M.; Morin, P. Auger electron-ion coincidence studies to probe molecular dynamics. *J. Electron Spectrosc. Relat. Phenom.* **2004**, *141*, 171−181.
(36) Le Guen, K.; Céolin, D.; Guillemin, R.; Miron, C.; Leclercq, N.; Bougeard, M.; Simon, M.; Morin, P.; Mocellin, A.; Burmeister, F.; et al. Development of a four-element conical electron lens dedicated to high resolution Auger electron−ion(s) coincidence experiments. *Rev. Sci. Instrum.* **2002**, *73* (11), 3885−3894.
(37) Liu, X.-J.; Nicolas, C.; Miron, C. Design of a lens table for a double toroidal electron spectrometer. *Rev. Sci. Instrum.* **2013**, *84*, 033105.
(38) Coville, M.; Thomas, T. D. Sulfur 2p ionization energies of H2S, OCS, SO2, and CS2. *J. Electron Spectrosc. Relat. Phenom.* **1995**, *71*, 21−23.
(39) Prümper, G.; Ueda, K. Electron-ion-ion coincidence experiments for photofragmentation of polyatomic molecules using pulsed electric fields: Treatment of random coincidences. *Nucl. Instrum. Methods Phys. Res., Sect. A* **2007**, *574*, 350−362.
(40) Eland, J. H. D.; Hochlaf, M.; Linusson, P.; Andersson, E.; Hedin, L.; Feifel, R. Triple ionization spectra by coincidence measurements of double Auger decay: The case of OCS. *J. Chem. Phys.* **2010**, *132*, 014311.
(41) Hikosaka, Y. Metastability and fragmentation of the OCS3+ states produced by S 2p double Auger decay. *J. Chem. Phys.* **2023**, *158*, 214306.
(42) Eland, J. H. D. Dynamics of Fragmentation Reactions From Peak Shapes in Multiparticle Coincidence Experiments. *Laser Chem.* **1991**, *11*, 259−263.
(43) Eland, J. H. D. The dynamics of three-body dissociations of dications studied by the triple coincidence technique PEPIPICO. *Mol. Phys.* **1987**, *61*, 725−745.
(44) Singh, R. K.; Lodha, G. S.; Sharma, V.; Prajapati, I. A.; Subramanian, K. P.; Bapat, B. Triply charged carbon dioxide molecular ion: Formation and fragmentation. *Phys. Rev. A* **2006**, *74*, 022708.
(45) Baker, C.; Turner, D. W. High resolution molecular photoelectron spectroscopy. III. Acetylenes and aza-acetylenes. *Proc. R. Soc. London A* **1968**, *308*, 19−37.
(46) Eland, J. H. D.; Squibb, R. J.; Sterling, A. J.; Wallner, M.; Roos, A. H.; Andersson, J.; Axelsson, V.; Johansson, E.; Teichter, A.; Stranges, S.; et al. Double and Triple Ionisation of Isocyanic Acid. *Sci. Rep.* **2020**, *10*, 2288.
(47) Wang, P.; Vidal, C. R.; Geith, J.; Klapötke, T. M.; Fuß, W. Dissociation of multiply ionized isocyanic acid through electron impact. *J. Chem. Phys.* **2004**, *120*, 123−128.
(48) Ruscic, B.; Berkowitz, J. The H-NCS bond energy, ΔH°_f (HNCS), ΔH°_f (NCS), and IP(NCS) from photoionization mass spectrometric studies of HNCS, NCS, and $(NCS)_2$. *J. Chem. Phys.* **1994**, *101*, 7975−7989.

https://doi.org/10.1021/acs.jpca.6c00386
J. Phys. Chem. A 2026, 130, 2602−2611